Applied Catalysis B: Environmental 201 (2017) 511–517

Contents lists available at ScienceDirect

Applied Catalysis B: Environmental

journal homepage: www.elsevier.com/locate/apcatb

Fabrication of direct Z-scheme Ta_3N_5-$WO_{2.72}$ film heterojunction photocatalyst for enhanced hydrogen evolution

Wan-Pyng Hsu [1], Mrinalini Mishra [1], Wei-Szu Liu, Chung-Yi Su, Tsong-Pyng Perng*

Department of Materials Science and Engineering, National Tsing Hua University, Hsinchu 300, Taiwan

ARTICLE INFO

Article history:
Received 25 March 2016
Received in revised form 27 June 2016
Accepted 26 August 2016
Available online 28 August 2016

Keywords:
Ta_3N_5
WO_3
Z-scheme
Atomic layer deposition
H_2 evolution

ABSTRACT

A combination of atomic layer deposition (ALD) and sol-gel techniques was applied to fabricate a direct Z-scheme Ta_3N_5-$WO_{2.72}$ heterojunction film photocatalyst for improved H_2 generation. The Ta_3N_5 was deposited by ALD on $WO_{2.72}$ sol coated on Si wafer. Ta_3N_5 film coated on bare Si wafer showed 13.2 μmol/g of H_2 generation after 6 h under irradiation by a 150 W Xe lamp with a cut-off filter (λ > 420 nm). In comparison, the direct Z-scheme Ta_3N_5-$WO_{2.72}$ heterojunction film demonstrated a more than two-fold increase in H_2 production (31.9 μmol/g). The efficiency of the Ta_3N_5-$WO_{2.72}$ heterojunction film further increased to 46.4 μmol/g upon coating with Pt nanoparticles by ALD. Additionally, the direct Z-scheme Ta_3N_5-$WO_{2.72}$ heterojunction film generated 18 times more H_2 than a Ta_3N_5-WO_3 liquid-state (using NaI as the shuttle redox mediator) Z-scheme system prepared by mixing Ta_3N_5 and WO_3 powders. The H_2 generation of the direct Z-scheme Ta_3N_5-$WO_{2.72}$ heterojunction film coated with Pt nanoparticles further increased to 3072.5 μmol/g without the 420 nm cut-off filter.

1. Introduction

Increasing energy consumption and demands, resulting in depletion of the primary energy resources, have led to various researches on photocatalytic [1] and photoelectrochemical [2] generation of H_2. The focus of the present study is to find photocatalysts which can tap the visible part of the solar spectrum as well as the UV part, along with being stable, non-toxic, abundant, and low cost.

Recently, Ta_3N_5 has emerged as a potential visible light photocatalyst [3]. The absorption edge of Ta_3N_5 is at 600 nm, corresponding to a band gap energy of about 2.1 eV [4]. This nitride semiconductor is stable and non-toxic, in contrast to other non-oxide semiconductors such as CdS [5] or CdSe [6]. It has a high theoretical solar-to-hydrogen (STH) conversion efficiency of 15.9% [7]. Further, Ta_3N_5 has suitable band edge positions for both H_2 and O_2 generation [8]. However, a single photocatalyst system poses problem of self-recombination of photo excited electrons and holes [9]. This can be overcome by combining with another semiconductor bearing suitable band edge positions based on the principle of Z-scheme system [10,11]. In Z-scheme, two different semiconductors separately suitable for H_2 and O_2 evolution are combined using an appropriate shuttle redox mediator. The mediator acts as an electron donor for the photogenerated holes in the valence band of H_2-evolution photocatalyst, thereby transforming into an electron acceptor, which in turn is reduced back to an electron donor by the photogenerated electrons in the conduction band of the O_2-evolution photocatalyst [10,11].

Several Z-scheme systems have been studied recently [10,11]. In particular, for Ta based nitrides, Tabata et al. demonstrated visible light-driven overall water splitting in an aqueous NaI solution by combining Pt/ZrO_2/TaON and Ir/R-TiO_2/Ta_3N_5 as H_2 and O_2 evolution photocatalysts, respectively [12]. Abe et al. reported enhanced H_2 evolution efficiency by applying the Z-scheme system constructed of Pt-loaded TaON and Pt-loaded WO_3 suspended in a NaI aqueous solution under visible light [13]. However, the presence of a shuttle redox mediator might decrease the efficiency of Z-scheme system due to undesirable competitive oxidation and reduction of the redox couples [14–18]. As a consequence, direct Z-scheme water splitting systems without a shuttle redox mediator are receiving increasing attention. In direct Z-scheme systems, the charges can transfer directly within the two semiconductors in physical contact to prevent the self-recombination [14–18]. The transfer mechanism of the photogenerated electrons and holes in the direct Z-scheme depends on the band edge positions of the two involved photocatalysts. Generally, the photogenerated electrons from the photocatalyst with higher conduction band edge migrate to the one with a lower conduction band edge position.

* Corresponding author.
E-mail address: tpperng@mx.nthu.edu.tw (T.-P. Perng).
[1] These authors contributed equally to this work.

http://dx.doi.org/10.1016/j.apcatb.2016.08.060
0926-3373/

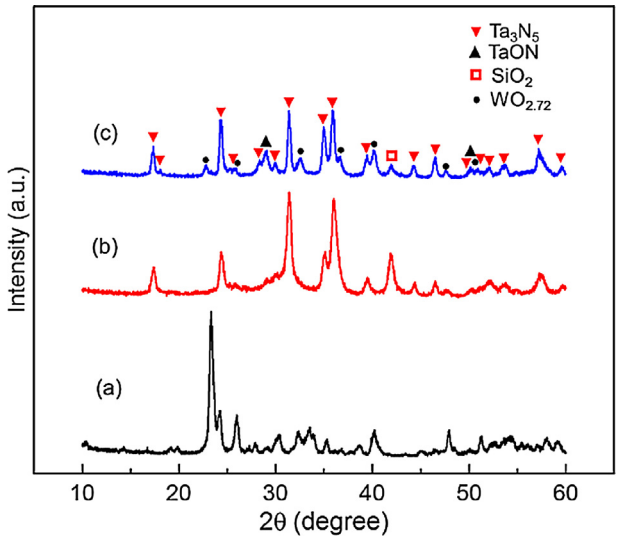

Fig. 1. GI-XRD patterns of (a) $WO_{2.72}$, (b) Ta_3N_5 thin film, and (c) Ta_3N_5-$WO_{2.72}$ heterojunction thin film heated to 900 °C by RTA in Ar.

Simultaneously, the photogenerated holes would migrate from the photocatalyst with lower valence band edge to the one with higher valence band edge position. However, in some cases, the photogenerated electrons in the photocatalyst with lower conduction band edge combine with the photogenerated holes in the photocatalyst with higher valence band edge position [19].

As mentioned earlier, it is necessary to have a suitable O_2-evolution photocatalyst with the H_2-evolution photocatalyst to work as a Z-scheme. In this work, Ta_3N_5 was used as the H_2-evolution photocatalyst along with WO_3 as the O_2-evolution photocatalyst [20]. The relative band edge positions of Ta_3N_5 and WO_3, are suitable for separation of the photo-generated charge carriers. Heterojunction of Ta_3N_5-WO_3 films on Si was fabricated as a direct Z-scheme system. This was achieved by using a combination of sol-gel and ALD techniques. The sol-gel method enables low processing temperature and control of particle size in the nanoscale [21]. ALD provides an ability to precisely control the composition and thickness of the layers, and can deposit extremely conformal and ultrathin film on substrates at relatively low operating temperatures [22] compared to other chemical or physical methods. Furthermore, Pt nanoparticles were also deposited by ALD to serve as an electron acceptor for the half-reaction of water reduction to form hydrogen [23–25]. For comparison, a liquid-state Z-scheme was constructed from a mixture of Ta_3N_5 and WO_3 powders synthesized by facile sol-gel method. In this liquid-state Z-scheme system, NaI was used as a redox mediator and Pt nanoparticles were also loaded by ALD.

2. Experimental

2.1. Fabrication of Ta_3N_5-WO_3 Z-schemes

To prepare the direct Z-scheme system, WO_3 and Ta_3N_5 films were fabricated on Si wafer. First, WO_3 sol prepared from 0.1 g of WCl_6 dissolved in 50 mL of 98% C_2H_5OH, was drop-coated on Si wafer and dried at 250 °C for 2 h. Then, the Ta_3N_5 film was deposited on WO_3 by 400 cycles of ALD. For ALD of Ta_3N_5, pentakis(dimethylamino)tantalum(V) (PDMAT) and NH_3 gas were selected as the precursors for tantalum and nitrogen, respectively. The growth temperature was set at 250 °C, and the pipe temperature was kept at 100 °C to prevent condensation of the precursor. The working pressure was set at 1 Torr, and each cycle consisted of a PDMAT pulse for 2 s and NH_3 pulse for 2.5 s which were separated by a N_2 purge for 10 s. The principle and setup for the ALD process have been presented previously [26,27].

In order to fix the temperature of crystallization, WO_3 sol and Ta_3N_5 films coated separately on bare Si wafers were heated in Ar ambience to 800, 900, and 1000 °C with a heating rate of 20 °C/s by rapid thermal annealing (RTA). Crystallization of the heterojunction film was then conducted by RTA in Ar ambience to 900 °C with the heating rate of 20 °C/s without holding time. Pt was deposited on Ta_3N_5-WO_3 heterojunction by 50 cycles of ALD. The ALD process for deposition of Pt nanoparticles has been reported earlier [28,29].

For fabricating the liquid-state Z-scheme system, Ta_3N_5 and WO_3 powders were synthesized by sol-gel method separately from tantalum chloride ($TaCl_5$) and tungsten chloride (WCl_6) precursors, respectively. 0.1 g of $TaCl_5$ or 0.1 g of WCl_6 was dissolved in 50 mL of 98% C_2H_5OH. After magnetically stirring for 2 h, the oxide sol was placed on a hot plate to evaporate out the solution and residual organics. The as-synthesized amorphous Ta_2O_5 and WO_3 powders were nitridized in NH_3 at 600–800 °C for 2 h with a flow rate of 150 sccm and calcined at 400–800 °C for 2 h in air, respectively, to obtain the optimal crystalline phases. Ta_3N_5 and WO_3 were then physically mixed at a molar ratio of 1:1.

2.2. Characterization of the Ta_3N_5-WO_3 Z-schemes

The amounts of WO_3 and Ta_3N_5 deposited on the Si wafer were measured by a 5-digit precision balance (Mettler Toledo). The crystallinity of the Ta_3N_5 films on bare Si wafer was identified by grazing incidence X-ray diffraction (GI-XRD, Rigaku-TTRAX III), with the incident angle of X-ray set at 0.5°. The Ta_3N_5 and WO_3 powders were examined by X-ray diffraction (XRD, Shimadzu XRD-6000). The morphologies of the heterojunction film and Ta_3N_5 and WO_3 powders were characterized by field emission scanning electron microscopy (FESEM) (Hitachi SU-8010). Elemental mapping was conducted using the energy dispersive X-ray (EDX) spectroscope attached to the FESEM. Morphological observation and EDX analysis were also performed by a JEOL JEM-3000F high resolution transmission electron microscope (HRTEM) operated at 300 kV. The specimen for HRTEM analysis was prepared by focused ion beam micromachining.

The surface elemental compositions and electronic states of elements of the heterojunction film samples were analyzed by X-ray photoelectron spectroscopy (XPS) (PHI 5000 Versaprobe II, Ulvac PHI Inc.). Al anode was chosen as the source for X-ray, and Ar ion gun was employed for sputtering. The variation of composition from the surface to the interlayer of the heterojunction film on Si wafer was investigated by XPS depth profiling with 5 cycles of sputtering. Ultraviolet photoelectron spectroscopy (UPS) was performed using the same instrument with He I (21.22 eV) as the excitation source at an applied bias voltage of 5 eV for films fabricated on Si and heated by RTA at 900 °C in Ar. The UV–vis diffuse reflectance spectra (UV–vis DRS) of powders and films were analyzed by a U-4100 spectrophotometer, Hitachi. The films were fabricated on quartz substrate for UV–vis DRS analysis.

2.3. Photocatalytic water splitting

The photocatalytic efficiencies for water splitting of the film and powder samples were evaluated by using a homemade steel reaction cell (volume = 65 mL) with a quartz window (diameter = 6 cm) under a 150 W Xe lamp equipped with a cut-off ($\lambda \geq 420$nm) filter. To determine the amount of H_2 generated, the gas sampling port of the reaction cell was connected to a gas chromatograph (GC, Simadzu GC-2014) through a six-way valve and a 1 mL sampling loop as a closed gas circulation system.

For the direct Z-scheme system, a Ta_3N_5-WO_3 hetero junction film ($2 \times 2\,cm^2$) was fixed onto the steel wall inside the reaction

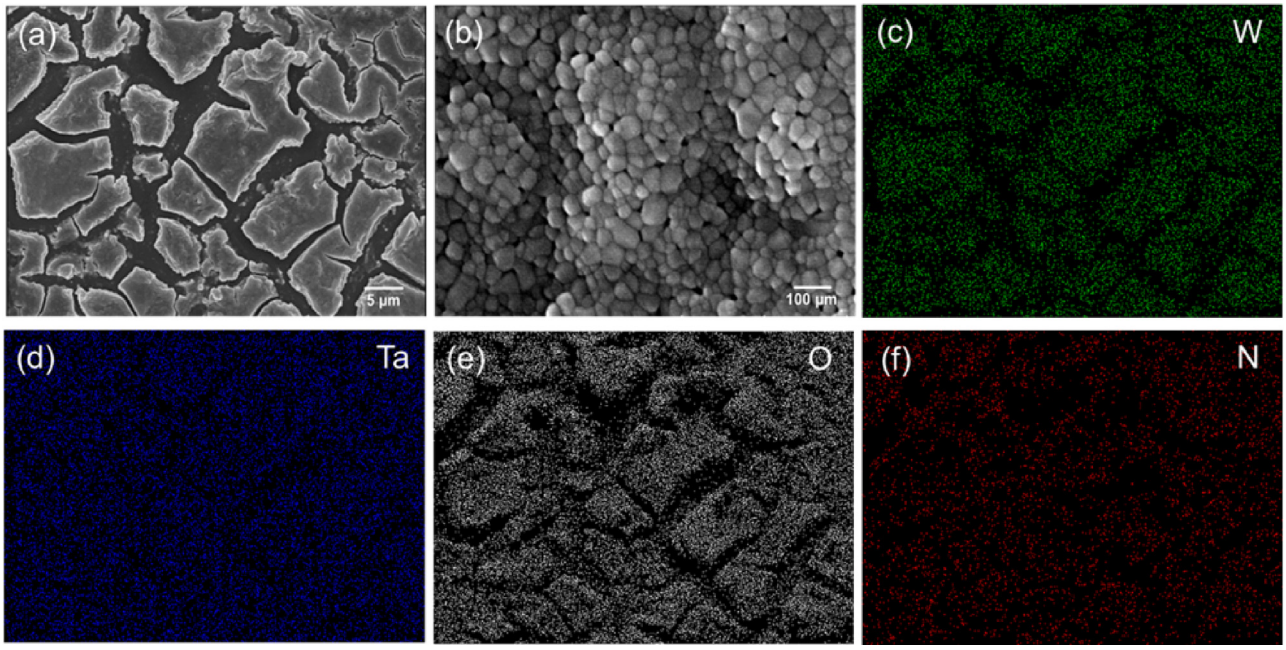

Fig. 2. Ta_3N_5-$WO_{2.72}$ heterojunction on Si after heating to 900 °C by RTA in Ar. (a) SEM micrograph, (b) higher magnification of (a). EDX mappings of (c) W, (d) Ta, (e) O, and (f) N.

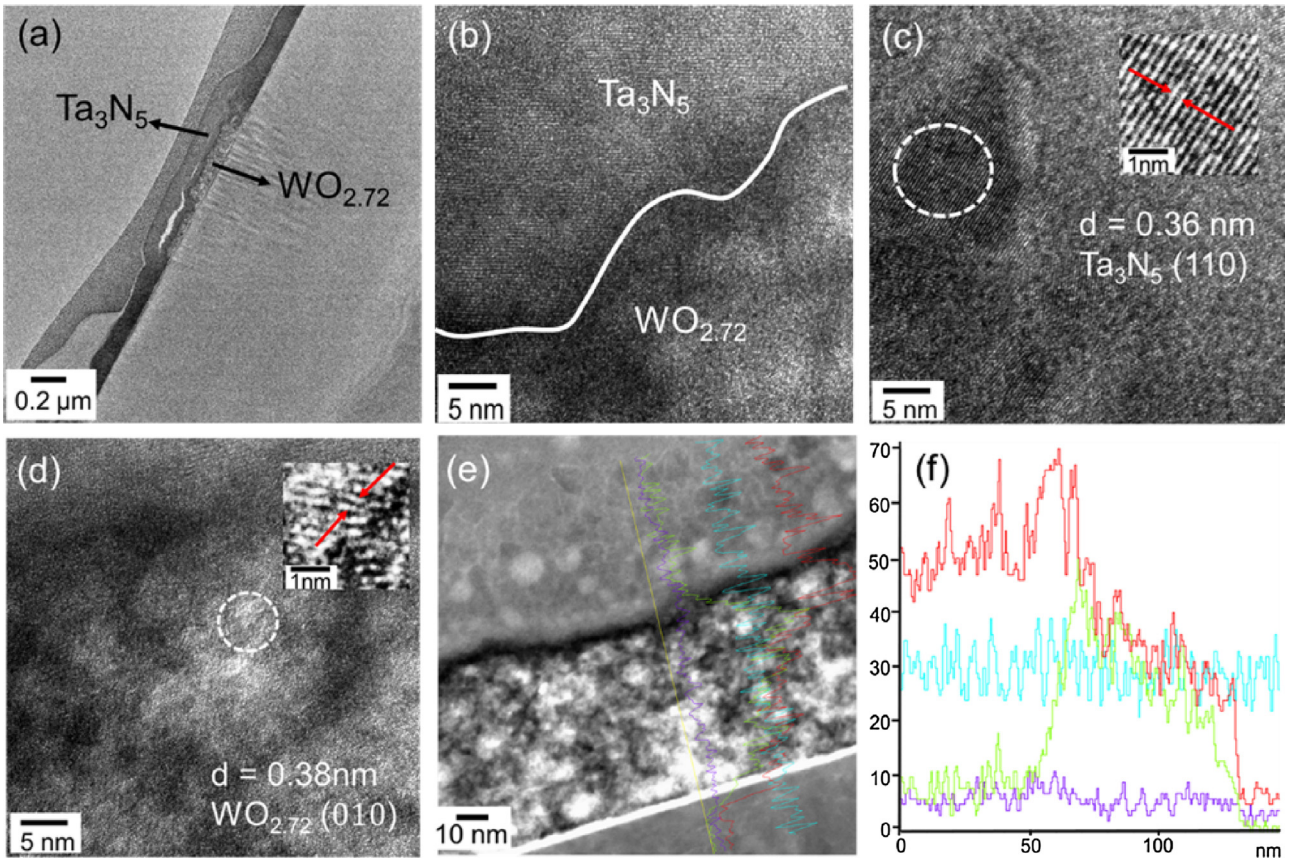

Fig. 3. Ta_3N_5-$WO_{2.72}$ heterojunction on Si after heating to 900 °C by RTA in Ar. (a) TEM micrograph, (b) higher magnification of (a). HRTEM micrographs of (c) Ta_3N_5 and (d) $WO_{2.72}$ layers. (e) and (f) are electron image and EDX line scan of the heterojunction showing signals of Ta in red, W in green, O in violet, and N in blue.(For interpretation of the references to colour in this figure legend, the reader is referred to the web version of this article.)

cell facing the Xe lamp. The reaction cell was then filled with 25 mL aqueous methanol solution (20 vol%) which acts as the sacrificial reagent. In case of the liquid-state Z-scheme system, the 1:1 molar mixture of Ta_3N_5 (0.02 g) and WO_3 (0.076 g) powders was dispersed in 25 mL aqueous methanol solution (20 vol%). NaI was added as the shuttle redox mediator (I^-/IO_3^-). Its concentration was fixed at 5×10^{-4} M in the reaction suspension.

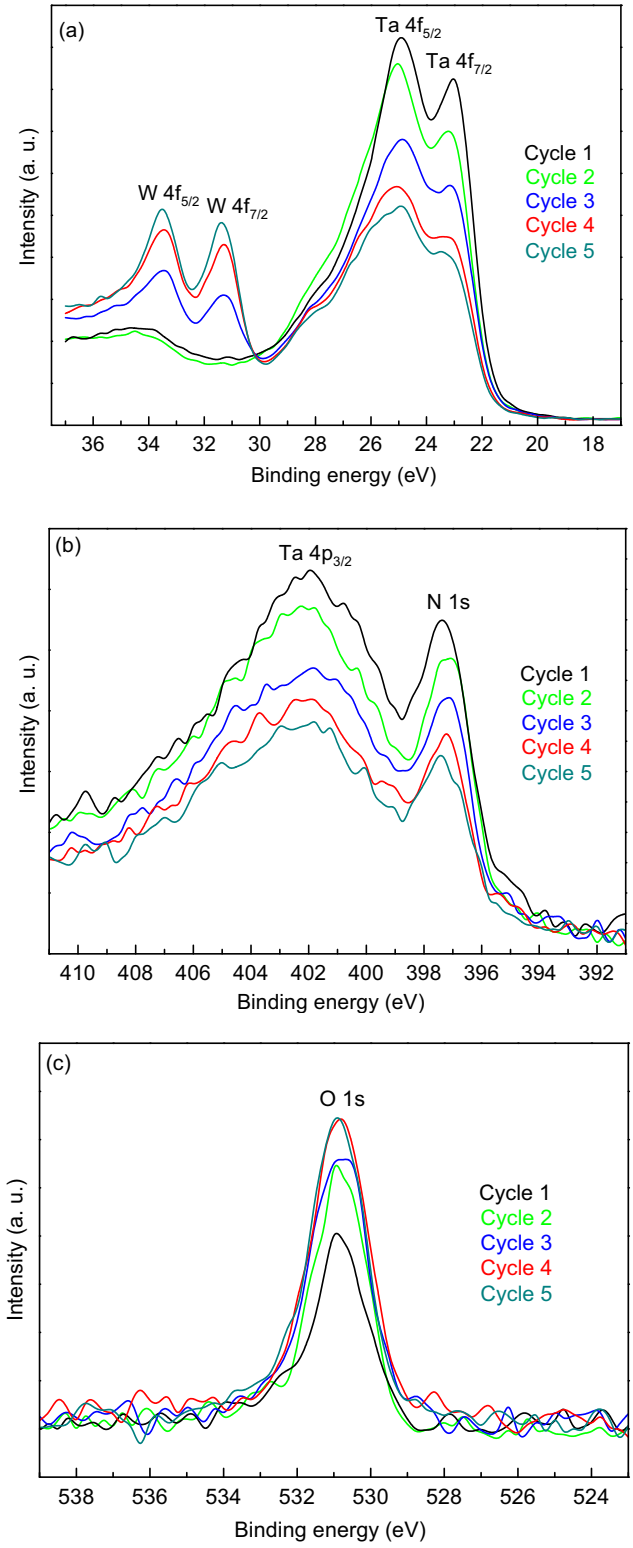

Fig. 4. XPS depth profile spectra for Ta_3N_5-$WO_{2.72}$ heterojunction on Si with 5 cycles of sputtering. (a) W 4f and Ta 4f, (b) Ta $4p_{3/2}$ and N 1 s and (c) O 1 s.(For interpretation of the references to colour in this figure legend, the reader is referred to the web version of this article.)

To ensure complete removal of air from the reaction cell, it was purged with Ar for 1 h before irradiation. Upon irradiation, GC readings were obtained every 1 h for 6 h to estimate the amount of H_2 evolved.

3. Results and discussion

3.1. Characterization of Ta_3N_5-$WO_{2.72}$ heterojunction film

For the direct Z-scheme heterojunction film on Si wafer, the weights of Ta_3N_5 and WO_3 were measured to be 4.7×10^{-4} g and 1.4×10^{-3} g, respectively, corresponding to a molar ratio of ~1:8. The average particle size of Pt deposited on the heterojunction film was ~2.4 nm, and the loading of Pt was estimated to be in the order of 1 μg/cm^2, based on our previous studies [28–30]. Fig. 1 displays the XRD patterns of as-deposited films heated to 900 °C by RTA in Ar without holding time. A sub-stoichiometric phase $WO_{2.72}$ was formed upon heating the WO_3 sol coated on Si wafer. This could be ascribed to the formation of oxygen vacancies in the material during the RTA process [31]. Nevertheless, $WO_{2.72}$ is well ordered and can be considered to be close to the WO_3 phase [32]. Crystalline phase of Ta_3N_5 was obtained when the as-deposited film was heated to 900 °C. Crystallinity improved further upon raising the temperature to 1000 °C, however, some minor TaON peaks also appear (Fig. S1). The (200) reflection from SiO_2 interlayer at 42° was detected due to the interaction of residual O_2 in the RTA chamber with the (100) oriented Si substrate during annealing. The heterojunction film was composed of $WO_{2.72}$ and Ta_3N_5 along with some very minor peaks of TaON and SiO_2.

Fig. 2(a) shows the morphology of Ta_3N_5-$WO_{2.72}$ heterojunction on Si after heating by RTA to 900 °C in Ar. It is seen that the heterojunction on Si wafer consists of many islands. TheWO_3 layer which was fabricated by drop-coating the sol on Si dries up to form island-like morphology. The higher magnification in Fig. 2(b) shows that each island is composed of numerous aggregated nanoparticles. EDX mapping shown in Fig. 2(c)–(f) confirms that the Ta_3N_5-$WO_{2.72}$ heterojunction on Si after RTA is composed of Ta, N, W, and O. The signals of W and O follow the morphology of island structure, and Ta_3N_5 appears to be deposited everywhere without any selectivity.

Fig. 3(a) shows the low magnification TEM image of the heterojunction on Si. The interface between the two photocatalysts as seen in the higher magnification TEM image shown in Fig. 3(b) illustrates a close and conformal contact. The d-spacings were found to be 0.36 nm and 0.38 nm for Ta_3N_5 (110) and $WO_{2.72}$ (010), respectively, as shown in Fig. 3(c) and (d). Fig. 3(e) and (f) depicts the EDX line scans of the heterojunction. The signal for Ta (red) is high in the Ta_3N_5 layer and drops down significantly in the $WO_{2.72}$ layer, while the signal for W (green) is high in the $WO_{2.72}$ layer.

The XPS depth profiles of Ta_3N_5-$WO_{2.72}$ heterojunction on Si subjected to 5 cycles of sputtering are shown in Fig. 4. The signals from the surface are mainly Ta and N. As the sputtering cycle is increased, the outer layer of Ta_3N_5 thins out and the peak intensities of W and O become stronger, while those of Ta and N gradually decrease as the $WO_{2.72}$ layer is approached. Thus, it is confirmed that the heterojunction is indeed composed of tantalum nitride and tungsten oxide.

The UPS is a reliable technique for determining the work function (φ) and band edges of semiconductor photocatalysts. Knowledge of work function and band edges help to critically assess the formation of Z-scheme [33,34]. The UPS spectra, as depicted in Fig. 5(a) and (b), were analyzed to determine φ for $WO_{2.72}$ and Ta_3N_5, respectively. The secondary cut-off region (E_{cut}) and Fermi energy level (E_F) could be clearly demarcated by intersecting lines. The values of φ were calculated from the equation $\varphi = h\nu - E_{cut} + E_F$, where $h\nu$ (21.22 eV) is the incident photon energy from the He I source and φ for $WO_{2.72}$ and Ta_3N_5 are 4.21 eV and 5.46 eV, respectively. These results suggest that electrons would transfer from the conduction band of $WO_{2.72}$ to combine with the holes in the valence band of Ta_3N_5. This evidences the formation of a Z-scheme. The distances from the valence band edge levels to the Fermi energy levels were obtained by linear intersection as 2.60 eV

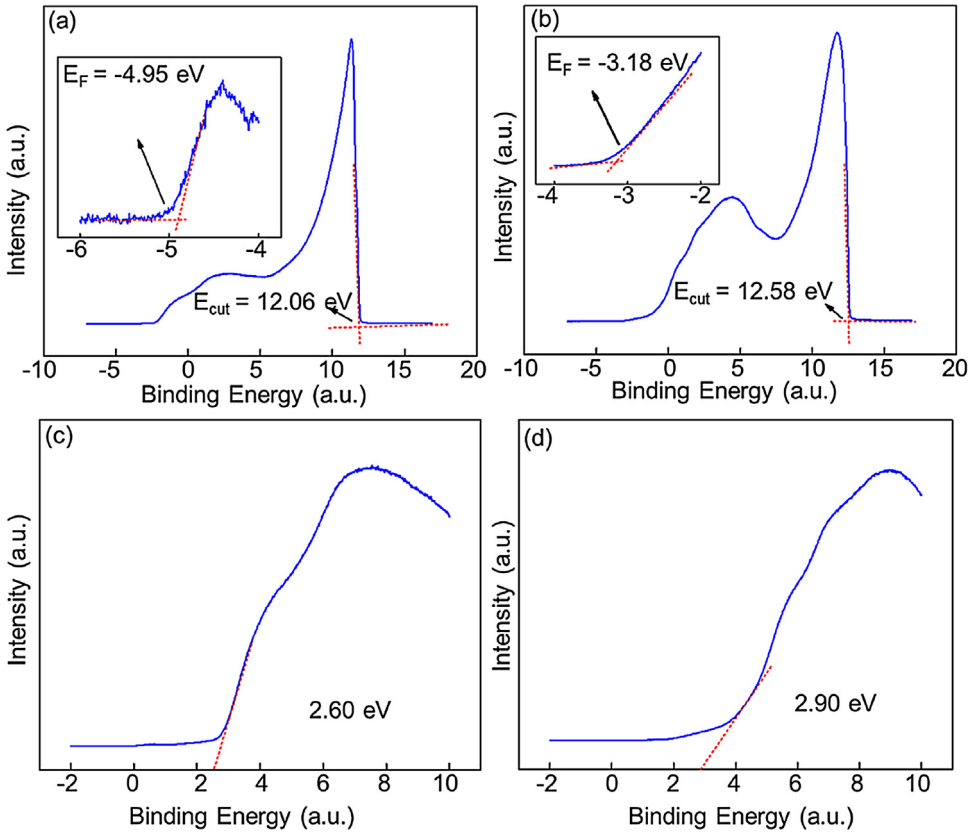

Fig. 5. UPS spectra of (a) $WO_{2.72}$ and (b)Ta_3N_5. The insets show magnified view of the Fermi level. Tangent lines are used to determine the Fermi level and secondary cut-off region. VB- XPS spectra of (c) $WO_{2.72}$ and (d) Ta_3N_5. Numbers in the figure are energy differences between the valence band edge levels and the Fermi levels.

and 2.90 eV for $WO_{2.72}$ and Ta_3N_5, respectively, from the VB-XPS spectra (Fig. 5(c) and (d)). The valence band levels ($E_{V.B.}$) were then calculated as −7.55 eV and −6.08 eV for $WO_{2.72}$ and Ta_3N_5, respectively. Subsequently, the conduction band levels were estimated via the equation $E_{C.B.} = E_{V.B.} + E_g$, to be −4.63 eV and −3.85 eV for $WO_{2.72}$ and Ta_3N_5, respectively. The values of E_g were calculated from the absorbance edges obtained by UV–vis DRS analysis, as described below.

The UV–vis DRS spectra (Fig. 6) show that the visible light absorbance of the Ta_3N_5-$WO_{2.72}$ heterojunction is enhanced compared to pure Ta_3N_5. However, the absorbance edge of the heterojunction appears to be shifted towards $WO_{2.72}$, probably due to its relatively higher molar content. It might also be influenced by the presence of small amount of TaON as seen in the XRD analysis (Fig. 1). The band gaps were estimated from the absorbance edges to be 2.92 eV, 2.23 eV, and 2.48 eV for $WO_{2.72}$, Ta_3N_5, and Ta_3N_5-$WO_{2.72}$ heterojunction, respectively. The band gap of $WO_{2.72}$ is in accordance with the reported value [35], whereas the band gap of Ta_3N_5 appears to be slightly blue-shifted. This band gap broadening could possibly be attributed to the presence of TaON and oxygen impurities. Harb et al. have shown by first principle calculations that oxygen enriched Ta_3N_5 has slightly broader band gap [36].

The details of the characterization of the Ta_3N_5 and WO_3 powders prepared for fabricating the liquid-state Z-scheme system are provided in the Supplementary information.

3.2. Hydrogen evolution from water splitting

Fig. 7displays the hydrogen evolution for various samples under 150 W Xe lamp (λ > 420 nm) over 6 h. Pure Ta_3N_5 film and Pt loaded Ta_3N_5 film directly deposited on Si wafer generate 13.2 μmol/g and 16.2 μmol/g of hydrogen in 6 h, respectively. Ta_3N_5 film modified by $WO_{2.72}$ to form the direct Z-scheme showed improved H_2 evolution (31.9 μmol/g of H_2 in 6 h). This improvement is 2.4 times of that of pure Ta_3N_5 thin film. Further, loading Pt nanoparticles as a co-catalyst resulted in even higher H_2 evolution (46.4 μmol/g in 6 h). In comparison, pure Ta_3N_5 powder and NaI mediated liquid-state Z-scheme system fabricated from Ta_3N_5 and WO_3 powders

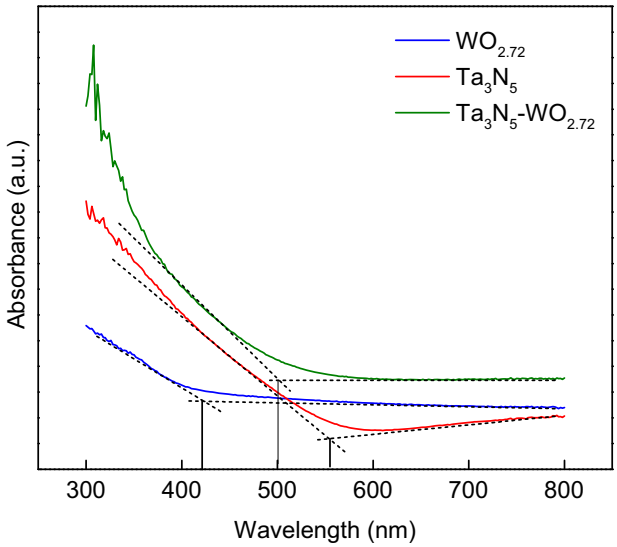

Fig. 6. UV–vis absorbance spectra of $WO_{2.72}$, Ta_3N_5, and Ta_3N_5-$WO_{2.72}$ heterojunction.(For interpretation of the references to colour in this figure legend, the reader is referred to the web version of this article.)

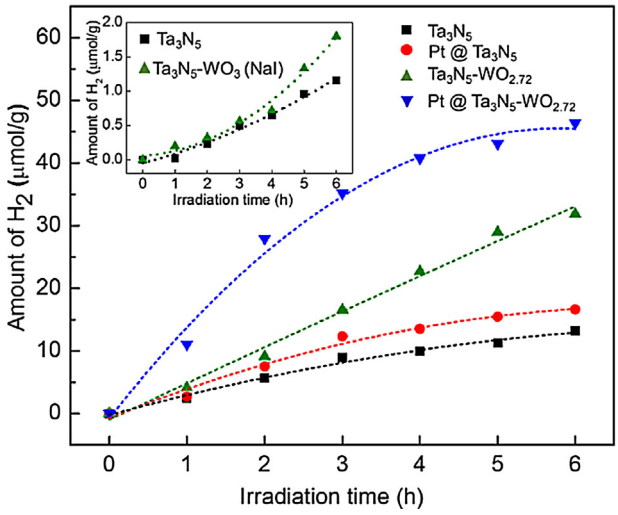

Fig. 7. Hydrogen evolutions by various film samples using a 150 W Xe lamp with filter ($\lambda \geq 420$nm). The inset shows hydrogen evolution by powder samples.

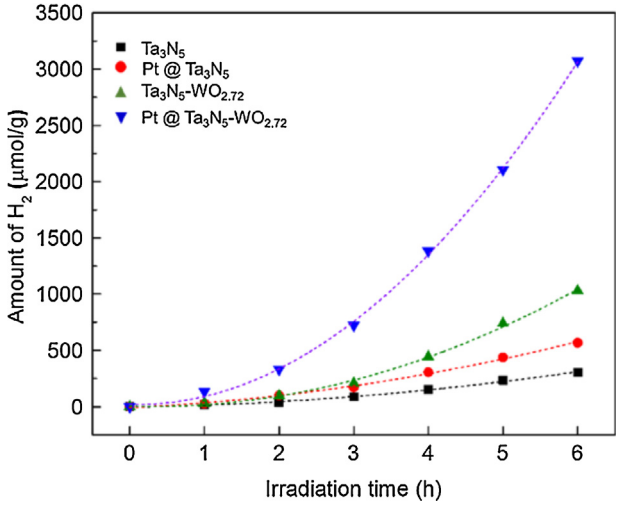

Fig. 8. Hydrogen evolutions by various film samples using a 150 W Xe lamp without filter.

yielded only 1.2 μmol/g and 1.8 μmol/g of H_2 in 6 h, respectively (inset of Fig. 7). The enhancement of H_2 evolution in the case of the liquid state Z-scheme system is inconsequential. In contrast, the direct Z-scheme Ta_3N_5-$WO_{2.72}$ heterojunction film photocatalyst yielded 18 times more than that of the redox couple mediated liquid-state Z-scheme system. It is clear that the conformal coating of Ta_3N_5 on $WO_{2.72}$ obtained by ALD facilitated good physical contact between the two photocatalysts, thereby easing the transfer of charges which is validated by the results of UPS analysis.

Hydrogen evolution for the direct Z-scheme Ta_3N_5-$WO_{2.72}$ heterojunction film was also studied under the whole spectrum of 150 W Xe lamp, i.e., without the filter ($\lambda > 420$ nm). Fig. 8 illustrates that after 6 h of irradiation the H_2 evolutions for Ta_3N_5 film and Ta_3N_5-$WO_{2.72}$ heterojunction film as photocatalyst reach 302.0 μmol/g and 1029.4 μmol/g, respectively. The H_2 production was further enhanced to 3072.5 μmol//g by applying Pt as co-catalyst on the heterojunction film. Hence, Pt assists the Ta_3N_5-$WO_{2.72}$ heterojunction synergistically for H_2 generation.

In retrospect, most of the reports on H_2 generation by Ta_3N_5 show application of co-catalysts like Pt [3,37]. In our work, we showed that, even without Pt co-catalyst, Ta_3N_5 thin films on bare and WO_3-coated Si wafers fabricated by ALD demonstrate significant H_2 production. Based on the results, a mechanism for water splitting by direct Z-scheme Ta_3N_5-$WO_{2.72}$ is proposed, as shown in Fig. 9. The photogenerated electrons in the conduction band of $WO_{2.72}$ bearing relatively lower work function easily migrate and recombine with the photogenerated holes in the valence band of Ta_3N_5, resulting in accumulation of photogenerated electrons in the conduction band of Ta_3N_5 that promote H_2 evolution. An interfacial electric field is generated in the direction of the electron transfer, which prohibits the transfer of electrons and holes between the conduction bands and valence bands, respectively, of the photocatalysts [34]. The generally accepted mechanism proposes that photogenerated electrons would migrate from the conduction band of Ta_3N_5 to that of $WO_{2.72}$. However, it does not apply to the results of this work as in that case H_2 production would not be possible since the conduction band edge of $WO_{2.72}$ is more negative than the reduction potential of water.

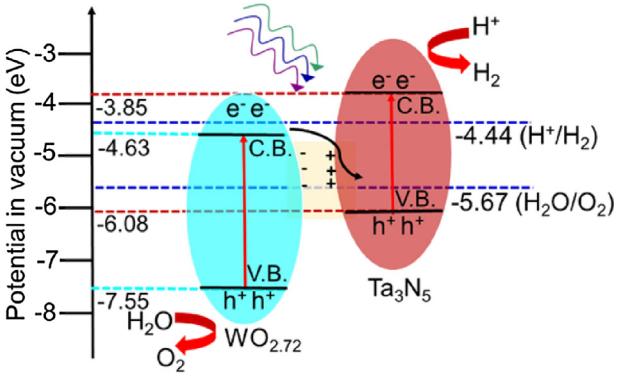

Fig. 9. Proposed Z-scheme mechanism for charge transfer processes with relative energy band positions of $WO_{2.72}$ and Ta_3N_5.

4. Conclusion

The Ta_3N_5-$WO_{2.72}$ heterojunction film fabricated by a combination of sol-gel and ALD techniques can be regarded as a promising photocatalyst for H_2 generation. A significant improvement in H_2 production is observed for the direct Z-scheme Ta_3N_5-$WO_{2.72}$ heterojunction film over liquid-state Z-scheme system constructed from the respective powders using NaI as the redox mediator. The present results demonstrate the possibility of applying ALD for fabricating efficient direct Z-scheme systems.

Acknowledgments

This work was supported by the Ministry of Science and Technology of Taiwan under Contract Nos. MOST 103-2120-M-007-005 and MOST 104-2119-M-007-010. The authors are thankful to Mr. Shih-Yuan Wei for UV–vis DRS measurement, Mr. Sheng-Hsin Huang for TEM characterization, and Mr. Vitaly Gurylev for thoughtful discussion.

Appendix A. Supplementary data

Supplementary data associated with this article can be found, in the online version, at http://dx.doi.org/10.1016/j.apcatb.2016.08.060.

References

[1] K. Domen, S. Naito, M. Soma, T. Onishi, K. Tamaru, Chem. Soc. Chem. Commun. 12 (1980) 543–544.
[2] A. Fujishima, K. Honda, Nature 238 (1972) 37–38.
[3] P. Zhang, J. Zhang, J. Gong, Chem. Soc. Rev. 43 (2014) 4395–4422.

[4] H.X. Dang, N.T. Hahn, H.S. Park, A.J. Bard, C.B. Mullins, J. Phys. Chem. C 116 (2012) 19225–19232.
[5] K. Kalyanasundaram, E. Borgarello, D. Duonghong, M. Grätzel, Angew. Chem. Int. Ed. 20 (1981) 987–988.
[6] M.A. Holmes, T.K. Townsend, F.E. Osterloh, Chem. Commun. 48 (2012) 371–373.
[7] A.B. Murphy, P.R.F. Barnes, L.K. Randeniya, I.C. Plumb, I.E. Grey, M.D. Horne, J.A. Glasscock, Int. J. Hydrogen Energy 31 (2006) 1999–2017.
[8] W.J. Chun, A. Ishikawa, H. Fujisawa, T. Takata, J.N. Kondo, M. Hara, M. Kawai, Y. Matsumoto, K. Domen, J. Phys. Chem. B 107 (2003) 1798–1803.
[9] M. Ni, M.K.H. Leung, D.Y.C. Leung, K. Sumathy, Renew. Sustain. Energy Rev. 11 (2007) 401–425.
[10] K. Maeda, ACS Catal. 3 (2013) 1486–1503.
[11] A. Kudo, MRS Bull. 36 (2011) 32–38.
[12] M. Tabata, K. Maeda, M. Higashi, D. Lu, T. Takata, R. Abe, K. Domen, Langmuir 26 (2010) 9161–9165.
[13] R. Abe, T. Takata, H. Sugihara, K. Domen, Chem. Commun. 30 (2005) 3829–3831.
[14] Y. Sasaki, H. Nemoto, K. Saito, A. Kudo, J. Phys. Chem. C 113 (2009) 17536–17542.
[15] S.S.K. Ma, K. Maeda, T. Hisatomi, M. Tabata, A. Kudo, K. Domen, Chem. Eur. J. 19 (2013) 7480–7486.
[16] X. Wang, G. Liu, Z.G. Chen, F. Li, L. Wang, G.Q. Lu, H.M. Cheng, Chem. Commun. 23 (2009) 3452–3454.
[17] Q. Jia, A. Iwase, A. Kudo, Chem. Sci. 5 (2014) 1513–1519.
[18] L.J. Zhang, S. Li, B.K. Liu, D.J. Wang, T.F. Xie, ACS Catal. 4 (2014) 3724–3729.
[19] S. Chen, Y. Hu, L. Ji, X. Jiang, X. Fu, Appl. Surf. Sci. 292 (2014) 357–366.
[20] R.G. Bamwenda, K. Sayama, H. Arakawa, J. Photochem. Photobiol. A 122 (1999) 175–183.
[21] L.L. Hench, J.K. West, Chem. Rev. 90 (1990) 33–72.
[22] D. Riihelä, M. Ritala, R. Matero, M. Leskelä, Thin Solid Films 289 (1996) 250–255.
[23] R. Abe, K. Sayama, H. Arakawa, Chem. Phys. Lett. 371 (2003) 360–364.
[24] I. Tsuji, H. Kato, H. Kobayashi, A. Kudo, J. Am. Chem. Soc. 126 (2004) 13406–13413.
[25] K. Maeda, M. Higashi, D. Lu, R. Abe, K. Domen, J. Am. Chem. Soc. 132 (2010) 5858–5868.
[26] C.C. Wang, C.C. Kei, Y.W. Yu, T.P. Perng, Nano Lett. 7 (2007) 1566–1569.
[27] W.T. Chang, Y.C. Hsueh, S.H. Huang, K.I. Liu, C.C. Kei, T.P. Perng, J. Mater. Chem. A 1 (2013) 1987–1991.
[28] C. Liu, C.C. Wang, C.C. Kei, Y.C. Hsueh, T.P. Perng, Small 5 (2009) 1535–1538.
[29] Y.C. Hsueh, C.C. Wang, C.C. Kei, Y.H. Lin, C. Liu, T.P. Perng, J. Catal. 294 (2012) 63–68.
[30] C.Y. Su, Y.C. Hsueh, C.C. Kei, C.T. Lin, T.P. Perng, J. Phys. Chem. C 117 (2013) 11610–11618.
[31] Y.S. Kim, Sens. Actuators B 137 (2009) 297–304.
[32] J. Booth, T. Ekström, E. Iguchi, R.J.D. Tilley, J. Solid State Chem. 41 (1982) 293–307.
[33] W.J. Chun, A. Ishikawa, H. Fujisawa, T. Takata, J.N. Kondo, M. Hara, M. Kawai, Y. Matsumoto, K. Domen, J. Phys. Chem. B 107 (2003) 1798–1803.
[34] H. Li, T. Hu, R. Zhang, J. Liu, W. Hou, App. Catal. B 188 (2016) 313–323.
[35] X. Guo, X. Qin, Z. Xue, C. Zhang, X. Sun, J. Hou, T. Wang, RSC Adv. 6 (2016) 48537–48542.
[36] M. Harb, P. Sautet, Ela Nurlaela, P. Raybaud, L. Cavallo, K. Domen, J.M. Basset, K. Takanabe, Phys. Chem. Chem. Phys. 16 (2014) 20548–20560.
[37] E. Nurlaela, S. Ould-Chikh, M. Harb, S. del Gobbo, M. Aouine, E. Puzenat, P. Sautet, K. Domen, J.M. Basset, K. Takanabe, Chem. Mater. 26 (2014) 4812–4825.